SIXTH QUARTERLY REPORT

21 November 1965 - 20 February 1966

GASEOUS ELECTROLYTES FOR BATTERIES AND FUEL CELLS

by

S. Naiditch, Principal Investigator

Prepared for

NATIONAL AERONAUTICS AND SPACE ADMINISTRATION

Contract NAS 7-326

UNIFIED SCIENCE ASSOCIATES, INC.

626 south arroyo parkway

pasadena, california 91105

murray 1-3456

SIXTH QUARTERLY REPORT

21 November 1965 - 20 February 1966

GASEOUS ELECTROLYTES FOR BATTERIES AND FUEL CELLS

by

S. Naiditch, Principal Investigator

Prepared for

NATIONAL AERONAUTICS AND SPACE ADMINISTRATION

Contract NAS 7-326

UNIFIED SCIENCE ASSOCIATES, INC.

826 south arroyo parkway

pasadena, california 91105

murray 1-3486

NOTICE

This report was prepared as an account of Government sponsored work. Neither the United States, nor the National Aeronautics and Space Administration (NASA), nor any person acting on behalf of NASA:

(A) Makes any warranty or representation, expressed or implied, with respect to the accuracy, completeness, or usefulness of the information contained in this report, or that the use of any information, apparatus, method, or process disclosed in this report may not infringe privately owned rights; or

(B) Assumes any liabilities with respect to the use of, or for damages resulting from the use of any information, apparatus, method or process disclosed in this report.

As used above, "person acting on behalf of NASA" includes any employee or contractor of NASA, or employee of such contractor, to the extent that such employee or contractor of NASA, or employee of such contractor prepares, disseminates, or provides access to, any information pursuant to his employment or contract with NASA, or his employment with such contractor.

Requests for copies of this report should be referred to:

National Aeronautics and Space Administration
Office of Scientific and Technical Information
Attention: AFSS-A
Washington, D. C. 20546

TABLE OF CONTENTS

ABSTRACT

Studies of the electrochemical characteristics of the conductivity cell have been completed. These cells have been designed for investigations of dense gaseous electrolytic solutions. By the use of special techniques we are now able to fabricate such cells to a predetermined cell constant within 1%.

The running of cell 64 has been terminated at 50°C due to a failure in the pressure bomb during the second run. A large leak developed in the cooling system, resulting in an abrupt pressure drop which caused the cell to explode. This cell, which was short term stable to 1 ppm, was our best cell to date. Comparison of the data for this short second run with that of the first run shows that the cell was not only reversible but also reproducible. After storage for over one month most emfs were repeatable within ± 0.5% up to 50°C.

We have now prepared stable, reversible, and reproducible amalgam concentration cells. Using the knowledge gained in this we will, in the next quarter, return to the metal amalgam-insoluble metal halide electrodes used earlier in this program.

Because of the presence of small leaks, the bomb was rebuilt early in the quarter. The total leak rate was reduced to 0.3 atmospheres per hour at 300 atmospheres (4500 psia). The recent failure of the coolant line,which caused the destruction of cell 64, was apparently caused by electrochemical attack of the stainless steel coolant tubing by amalgam thrown against it when a cell ruptured during an earlier measurement.

1. CELL 64

The first run of cell 64 lasted 14 days and covered the temperature range from 13 to 100°C (Fig. 1). The second run lasted 5 days before the bomb failed. The cell preparation and first six days of the first run were covered in the fifth quarterly report.[1] For continuity, the entire set of data is presented in this report.

The data are presented in tables 1 and 2 and figures 2 and 3. Though we did not reach the critical temperature, past experience[2] and the current data lead us to expect that the emfs should extrapolate smoothly from 0.13 volts at 100°C to about 0.7 volts at 140°C.

Due to the large changes in their emf with temperature, electrodes B and D are of particular interest. At lower temperatures (25°C), there is an effective sodium activity ratio of about 10 between electrodes B and D; however, at 100°C, the ratio drops to nearly unity. When the cell was mounted in the bomb, inspection showed the appearance of the amalgams B and D to be similar. Both were in the liquid state and therefore of low concentrations. These gradual and reversible changes in activities can also be seen in several other electrode pairs. Looking at AC, AD, AB, one sees an increase in sodium activity in electrode A. Similarly, BC and BD show a decrease in that of B. Also, there are related marked changes in E/T between 75 and 100°C.

[1]Fifth Quarterly Report Contract NAS 7-326, p. 23-31.

[2]Fifth Quarterly Report Contract NAS 7-326, p. 21.

It was possible on cooling after the first run, to repeat most data points within 1%. This repeatability shows the changes were due to reversible effects and made it possible to continue these measurements after the pressure system was rebuilt.

After a storage period in excess of one month, the average changes in the emfs to 50°C were less than 0.5%.

This run was terminated by a bomb decompression caused by a cooling line failure. The cell rupture was so violent that the cell and its teflon bag were completely destroyed. Most of the cell was broken into pieces no larger than sand. The violence of this explosion made the gathering of amalgam samples for analysis impossible.

Though we have yet to run a stable concentration cell into the critical region, we now feel, due to the excellent stability and reversibility of cell 64, that we understand the cells well enough to return to metal amalgam-insoluble metal halide electrodes.

TABLE I. Cell 64 EMF Data from 13°C to 99.2°C

*	TEMP. °C	EMF, VOLTS					
		DA	DC	- DB	- AB	- AC	BC
3	13	0.100838	0.0142858	0.0183090	0.119139	0.0865855	0.0325720
4	14	0.100925	0.0142731	0.0183167	0.119224	0.0866800	0.0325635
6	18.5	0.101659	0.0142490	0.0179611	0.119584	0.0874139	0.0321958
5	25	0.100740	0.014430	0.0156810	0.11883	0.08553	0.033390
2	27	0.099825	0.014389	0.018635	0.11846	0.085480	0.033000
8	40.5	0.101900	0.0155299	0.018700	0.120490	0.0863122	0.0342105
7	41	0.101564	0.015530	0.0187354	0.120345	0.0861249	0.034268
10	56	0.10347	0.01639	0.01876	0.12220	0.08710	0.03512
9	56.5	0.10351	0.01642	0.01872	0.1223	0.08719	0.03513
12	62	0.10532	0.01653	0.01845	0.12372	0.08871	0.03490
11	73	0.10813	0.01737	0.01779	0.1259	0.09093	0.03510
13	99.2	0.1334	0.03028	0.00108	0.13439	0.1030	0.03130
14	74.5	0.1097	0.01749	0.01669	0.12633	0.09230	0.0349
15	20.3	0.104182	0.0144120	0.0169588	0.121156	0.089784	0.0313707
**							
16	21.9	0.0991012	0.0145817	0.0186099	0.117730	0.0845598	0.0331614
17	20.7	0.100762	0.0142180	0.0184985	0.119260	0.0865322	0.0327172
18	21.4	0.100480	0.0142328	0.0186057	0.119082	0.0862372	0.0328420
***							
19	20.0	0.101081	0.0140900	0.0183491	0.119559	0.0868465	0.0327146
20	20.9	0.101524	0.0141812	0.0185100	0.120008	0.0872752	0.0326940
21	41.9	0.101910	0.0152710	0.0188068	0.120627	0.086476	0.0341330
22	39.7	0.101694	0.0152135	0.0187758	0.120500	0.086516	0.0339847
23	51.3	0.10255	0.015769	0.01886	0.12131	0.08673	0.03453
24	49.7	0.10205	0.015693	0.01884	0.12086	0.086360	0.034512

*Order in which data were taken.
**Over one month storage at 0°C.
***Additional fifteen days storage at 0°C.

TABLE 2. Cell 64 E/T Data from 13°C to 99.2°C

*	TEMP. C	TEMP. °K	E/T, VOLTS $^{\circ}K^{-1}$					
			DA	DC	- DB	- AB	- AC	BC
3	13	286	3.52580×10^{-4}	4.99503×10^{-5}	6.40175×10^{-5}	4.16570×10^{-4}	3.02747×10^{-4}	1.13881×10^{-4}
4	14	287	3.51655	4.97321	6.38213	4.15415	3.02021	1.13462
6	18.5	291.7	3.48744	4.8882	6.16161	4.10237	2.99876	1.10449
5	25	298	3.38054	4.8423	5.26208	3.9876	2.870	1.12051
2	27	300	3.3275	4.7963	6.2116	3.9486	2.8493	1.1000
8	40.5	313.7	3.25040	4.95371	5.9649	3.84338	2.75318	1.09124
7	41	314	3.234522	4.9459	5.96669	3.83264	2.74283	1.0913
10	56	329	3.1450	4.982	5.702	3.7143	3.647	1.067
9	56.5	329.7	3.1414	4.983	5.681	3.712	2.646	1.066
12	62	335	3.1439	4.934	5.508	3.6931	2.648	1.042
11	73	346	3.1251	5.020	5.142	3.630	2.628	1.015
13	99.2	372.4	2.582	8.131	2.90	3.67087	2.765	0.8405
14	74.5	347.7	3.157	5.033	4.803	3.6354	2.656	1.004
15	20.3	293.5	3.55206	4.91314	5.78207	4.13079	3.0612	1.06958
16	21.9	295.1	3.3582	4.9412	6.3063	3.9895	2.8655	1.1237
17	20.7	293.9	3.4284	4.8376	6.2941	4.0574	2.94427	1.1132
18	21.4	294.6	3.4107	4.8312	6.3156	4.0422	2.9273	1.1148
19	20.0	293.2	3.4475	4.8056	6.2582	4.0777	2.9620	1.1158
20	20.9	294.1	3.4520	4.8219	6.2938	4.0805	2.9675	1.1117
21	41.9	315.1	3.2342	4.8464	5.9685	3.8282	2.7444	1.0832
22	39.7	312.9	3.2500	4.8621	6.0006	3.8511	2.7650	1.0861
23	51.3	324.5	3.1602	4.8595	5.8120	3.7384	2.6727	1.02641
24	49.7	322.9	3.1604	4.8600	5.8346	3.7429	2.6745	1.0688

*Order in which data were taken.

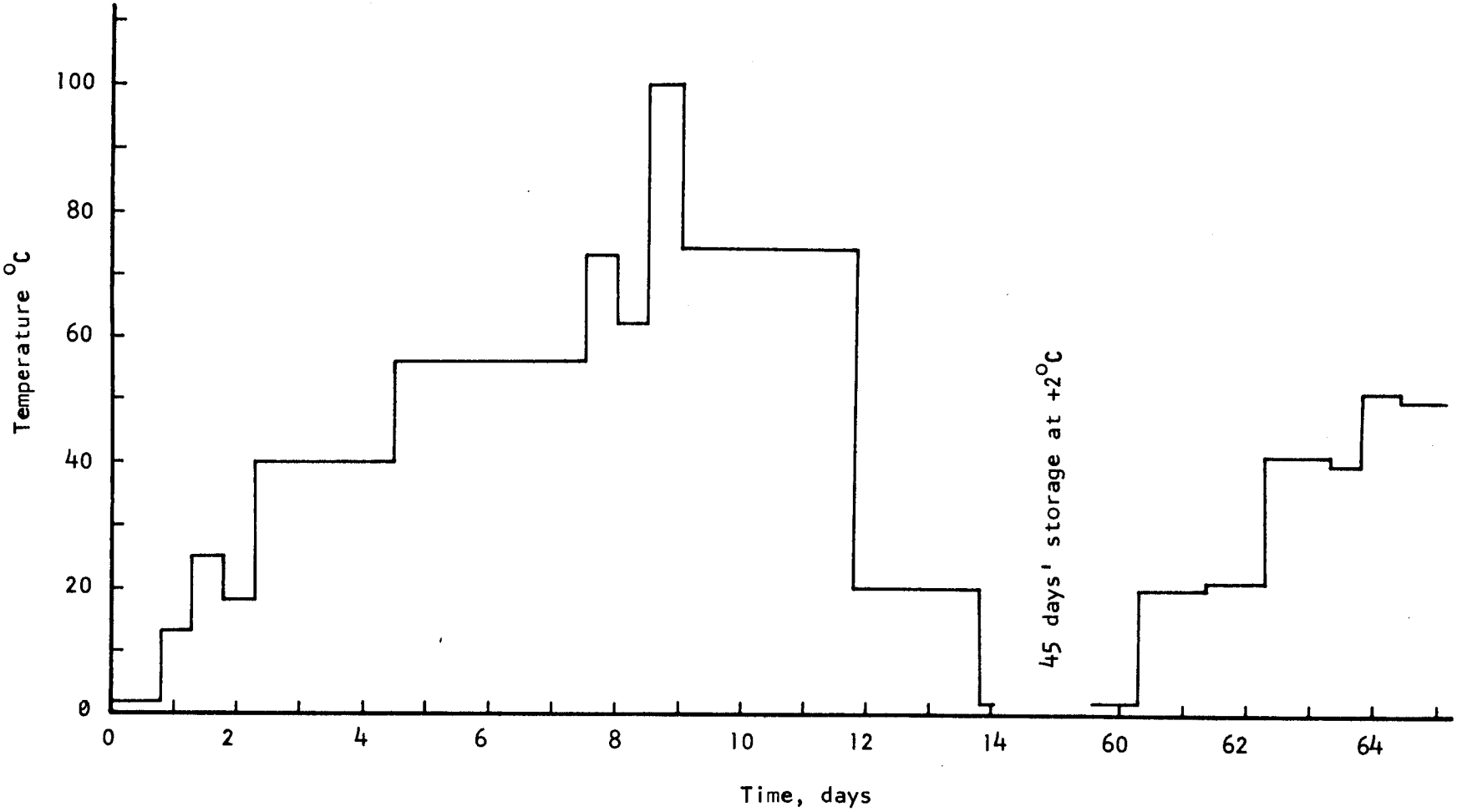

Figure 1. Temperature Cycle for Cell 64

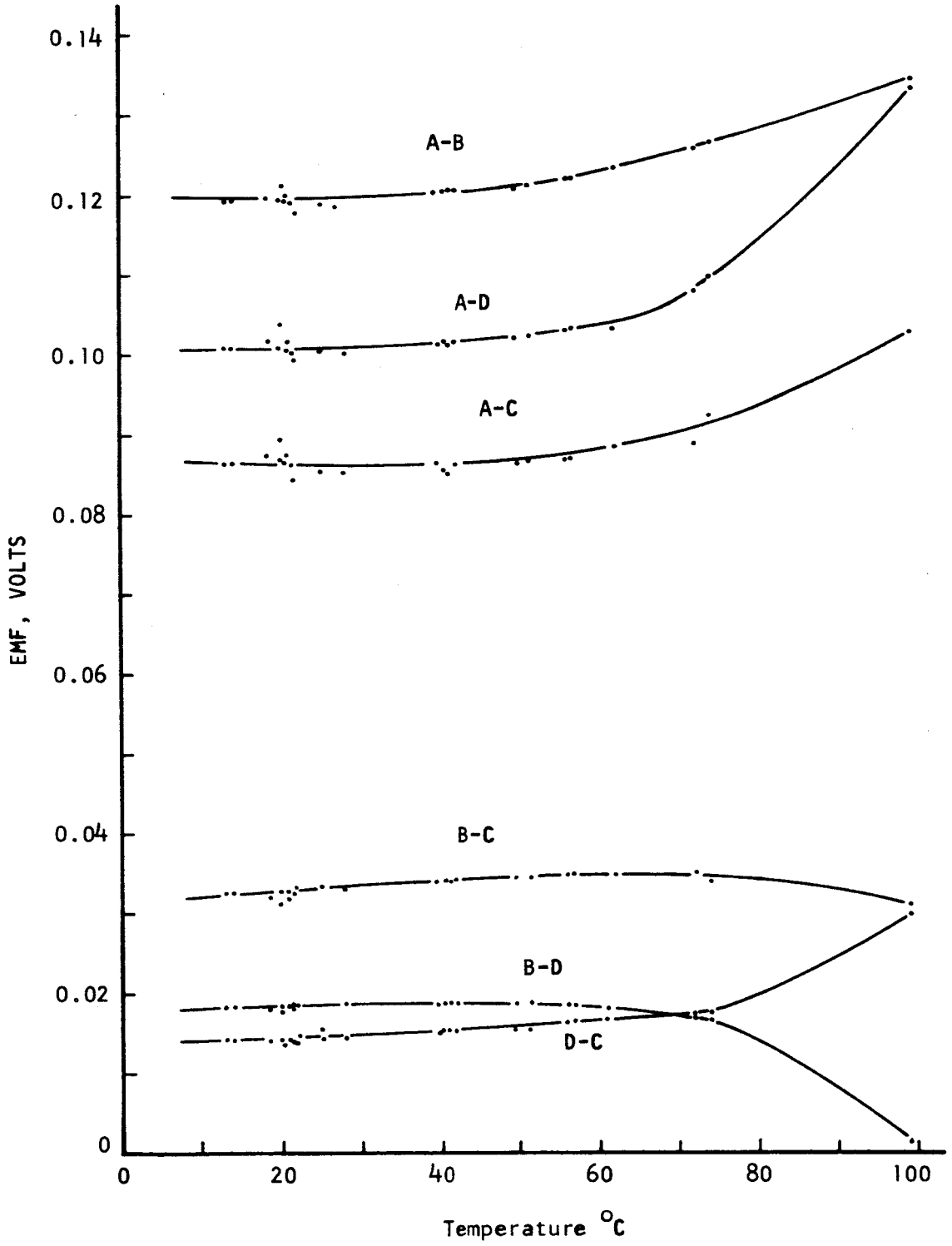

Figure 2. EMF Data for Both Runs of Cell 64.
Points from the first run are virtually indistinguishable from those of the second run.

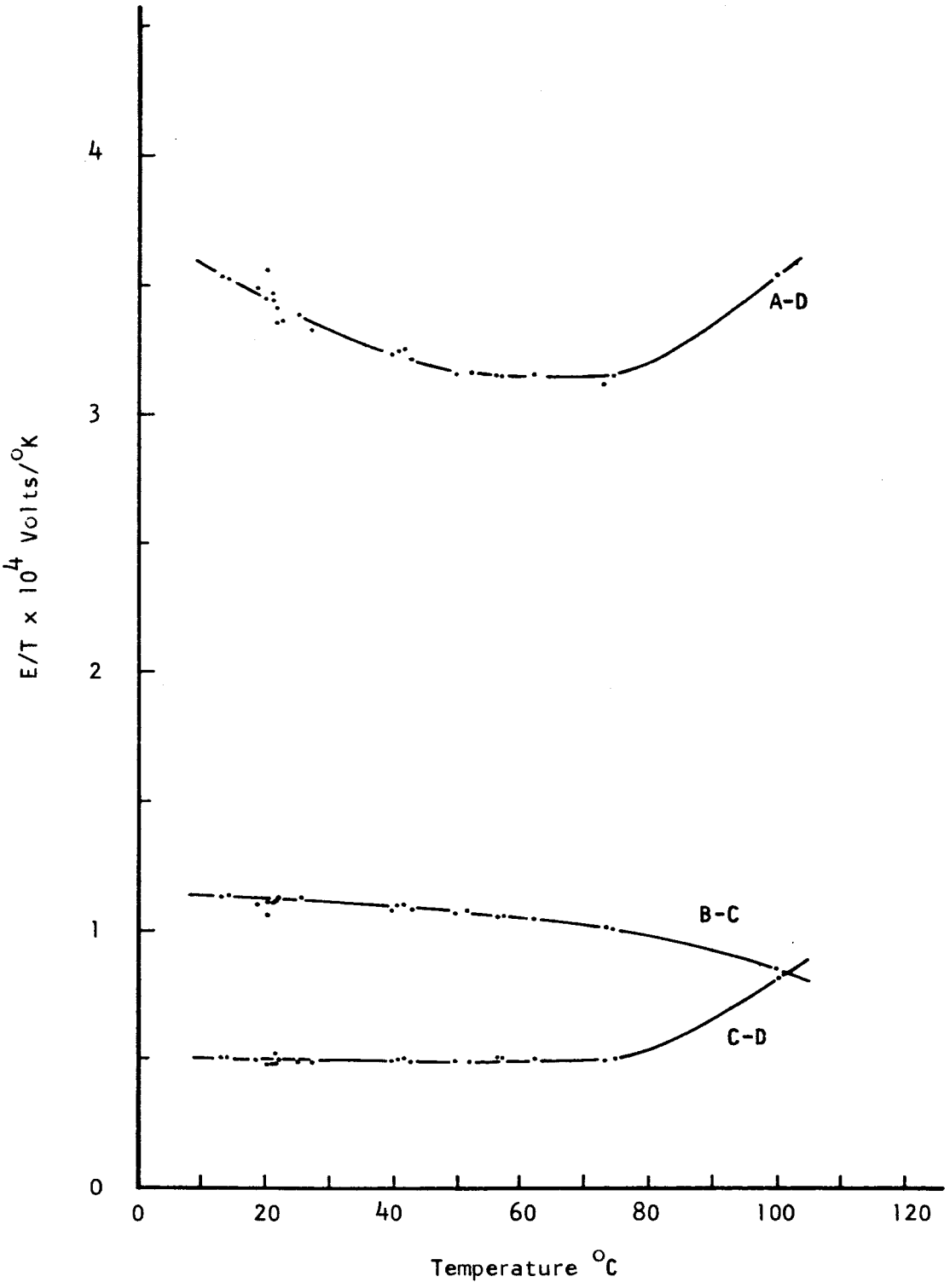

Figure 3. E/T Data for Cell 64

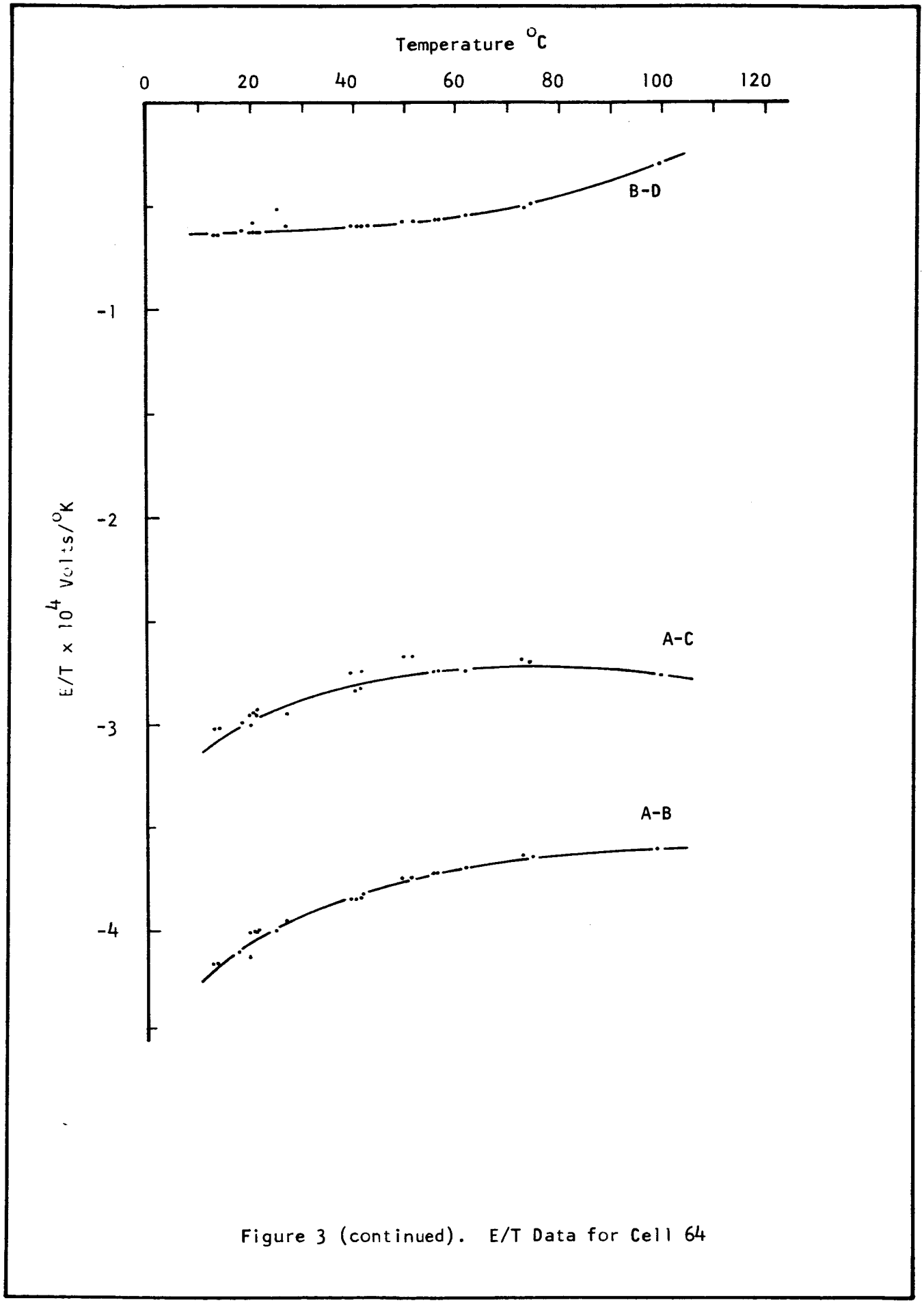

Figure 3 (continued). E/T Data for Cell 64

2. CHARACTERISTICS OF THE CONDUCTIVITY CELL

2.1 INTRODUCTION

This study was undertaken to build better cells for use in measuring the electrochemical properties of dense gaseous electrolytic solutions. Ammonia was chosen as the initial solvent, since it has relatively mild critical conditions, 112 atm at 132.9°C. Even so, standard glass cells are not usable under these pressures. Even cells of pyrex capillary tubing fail at the metal-to-glass seals (electrodes). The problem of constraining the high internal pressure can be circumvented by subjecting the cells to an even higher external pressure in a high pressure chamber.

The high pressure bomb has a 1-1/2" inside diameter which made the design of a special cell necessary. Due to this spatial restriction, it was apparent that the extraneous inductances and capacitances associated with a.c. would be difficult to eliminate. By using a four probe d.c. technique, we avoided the polarization problems affecting two probe d.c. measurements.

The principal factor leading to this more detailed study of cell characteristics was our inability to get quantitative agreement between cell constant measurements using mercury and those using KCl. As a result, we modified the cell construction so that we could determine the cell constants by geometric measurements as well as by a newly devised dip-rod technique.

Though the use of slit electrodes provides voltage averaging over the entire circumference of the slit, it also introduces distortion in the potential field due to the finite width of the slit. We have found that this distortion

disappears when the slit width is reduced to 0.1 mm or less. The cell constant is then a function only of conductivity tube length and area and not of the slit width.

With the techniques developed in this study, we are now able to fabricate cells to specified cell constants within 1%, using geometric measurements only. These cells are usable for studies of the electrochemistry of dense gaseous electrolytic solutions.

2.2 EXPERIMENTAL

2.2.1 Cell Design

The four-electrode cells used for our experiments are shown in Fig. 4. The two extreme electrodes are used to carry the current, and the two intermediate electrodes, to measure the voltage developed across the middle cylindrical section, which is called the "conductivity tube" in the following discussion. The side arms are used to facilitate the filling process, then sealed off so that the cell can be inserted into the pressure vessel. The factors on which the cell design is based are as follows:

a. The current density in the conductivity tube must be constant and uniform in the region of, and between, the two emf measuring slits. When this condition is satisfied, the cell constant K can be determined by geometrical measurements, being equal to L/A, the ratio of the length of tubing between the emf slits to the internal cross-sectional area of the conductivity tube.

b. The potential difference between the two ends of the conductivity tube is measured through the pair of narrow slit apertures perpendicular to and encompassing the entire circumferences of the conductivity tube. One reason that this geometry was selected, instead of the small circular hole as in a Luggin electrode, is that if there are any nonuniformities in the electrolyte or emf distribution, use of the circular emf measuring slit should average them out. That is, we scan or sample the emf over a complete equipotential instead of at a single locality. Secondly, for a

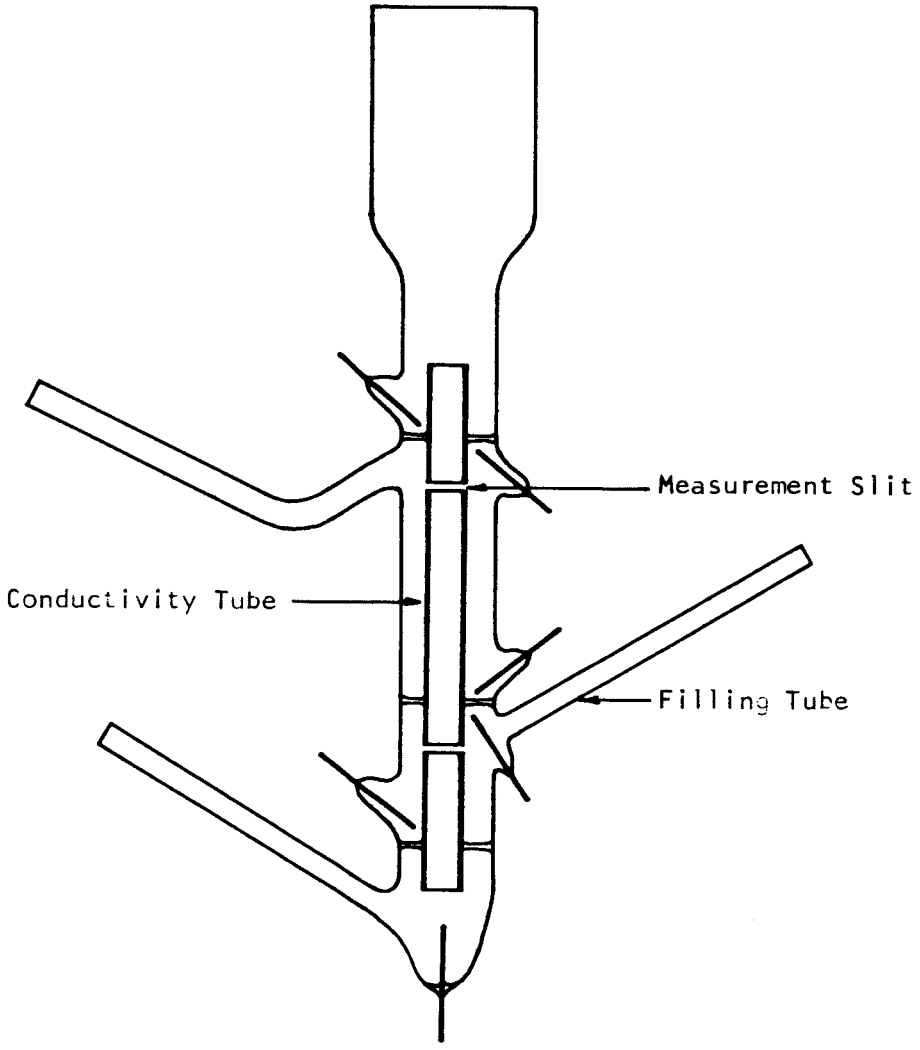

Figure 4. Special Cell for Studying the Cell Constant

given scanning area, a slit can be made narrower than a circular hole; therefore, the potential drop across the width of the slit and the cell impedance are less than across a hole. Under this condition, there is less penetration of the current into the emf measuring region.

c. The cross-sectional area of the conductivity tube must be uniform and constant along its entire length. Furthermore, in order to facilitate the determination of this area, the cross section should also be circular.

d. The sections of the conductivity tube must be sharply defined.

e. The cell should be able to withstand a compressive pressure differential of the order of 10 - 50 atmospheres.

f. The tungsten-pyrex graded seals used in the cell must not be weakened by the cell preparation procedure. We found that use of liquid nitrogen weakened this region, and led to frequent failures. For this reason, we placed a freeze cup above the main cell. The portion of the cell below the freeze cup is only subjected to dry ice-alcohol temperatures. By filling the freeze cup with liquid nitrogen, we form a solid plug of solvent which acts as a freeze valve. This allows us to evacuate the cell stem above this valve before sealing off.

2.2.2 Cell Fabrication - Internal

In order to fabricate a cell to meet the specifications, we had to place the mounting flange holding the conductivity tube an appreciable distance from either end. During the fabrication we found that in putting the glass flange on the outside of the conductivity tube, the tube was compressed during glassblowing so that its inside diameter, at that region, was about 2% smaller than that of the remainder of the tube. In addition, this flange has a tendency to crack, as was actually the case with several cells.

After experimenting with several fabrication techniques, we adopted the following. A piece of ordinary glass tubing closed at one end was collapsed over drill rod of the desired diameter by heating the tubing while maintaining a partial vacuum inside it. While the tube was hot and the drill rod still inside, the glass flange was built up on the tube at the desired location. By this method we were able to eliminate the compression problem entirely and simultaneously produce a tube of uniform and constant cross section with a glass flange from ordinary glass tubing.

Once the problem of producing precision bore glass tubing with flanges was solved, it became possible to make a cell with narrow voltage measurement slits. Three cells were fabricated with slit widths of 4 mm, 0.4 mm and 0.1 mm, to determine the effect of slit width on the cell constant.

In addition, for the purpose of checking whether the voltage across the conductivity tube is influenced by the positions of the voltage measurement leads, electrodes B1 and C1 were added in cell 74. It is to be noticed

that even with electrodes B2 and C2 below the slits, while electrodes B1 and C1 are located above these slits, no measurable emf (< 1 microvolt) was noted across B1-B2 and C1-C2 for slits less than 0.4 mm.

All leads in our cells are tungsten wires, sealed to the cell envelopes by means of standard tungsten-to-glass seals. All exposed tungsten surfaces inside the cell were platinized by melting a platinum wire onto the surfaces.

2.2.3 Measurement of the Cell Constant

Cell constants have been determined by three methods. The first of these is the geometric method in which the inside diameter of the conductivity tube is measured by means of a small hole gage and a micrometer, and its length is measured with a caliper before assembly and with a cathetometer after assembly. The cell constant is then computed from the equation $K = L/A$. It is necessary to introduce corrections for end effects for slit-widths greater than 0.01 cm.

The second method is also conventional. The cell constant is computed from the equation $K = R\sigma$, using the d.c. resistance measured across the conductivity tube and the known conductivity of the conducting liquid inside the cell. Both mercury and 1.0 N KCl solution are used as the conducting liquids.

In the third method, the cell is filled with a conducting liquid and a glass dip rod is inserted into the conductivity tube. The voltage is measured as a function of the position of the bottom of the rod. Graphically, we determined the slope S_x of voltage with respect to rod location at constant current.

$$\sigma = \frac{i}{S_x} \frac{A_r}{A_o(A_o - A_r)}$$

where A_o is the internal cross-sectional area of the conductivity tube, A_r is the cross-sectional area of the rod, and i is the (constant) current. The conductivity of the conducting liquid does not enter into this expression. If the expression is rewritten

$$\frac{dR}{dX} = \rho \frac{A_r}{A_o(A_o - A_r)}$$

it is seen that the term $\frac{A_r}{A_o(A_o - A_r)}$ is the cell constant for the variable dip rod technique.

In applying the dip-rod method to measure the cross-sectional area and length of the conductivity tube, and consequently the cell constant, it is important to measure accurately the depth of insertion of the dip rod into the conductivity tube. For convenience in making this series of measurements, a commercial drill press was used. The dip rod was mounted in the chuck of the drill head so as to provide vertical rod motion, and a cathetometer was mounted on the platform of the drill press to measure the travel of the rod. By this method we were able to move the dip rod up and down in the conductivity tube easily, while maintaining accurate vertical alignment, and to measure the amount of rod movement with an accuracy of ± 0.01 mm.

We accurately ground the outer surface of a glass rod for use as the dip rod. It has a diameter of 4.026 ± 0.004 mm over a length of approximately 5 cm., i.e., the length of the conductivity tube. (Surprisingly, precision glass rods are not listed in standard supply catalogs.)

2.3 CURRENT-VOLTAGE CHARACTERISTICS

Typical current-voltage curves are given in figures 5 and 6 for cell 66, which was built with ordinary pyrex tubing. Data are plotted for both Hg and 1 N KCl with and without a dip rod in the system.

The linearity of the current-voltage plots and the fact that the line goes through the point (0,0) indicates that the measuring system is well behaved with both Hg and KCl as the conducting fluids.

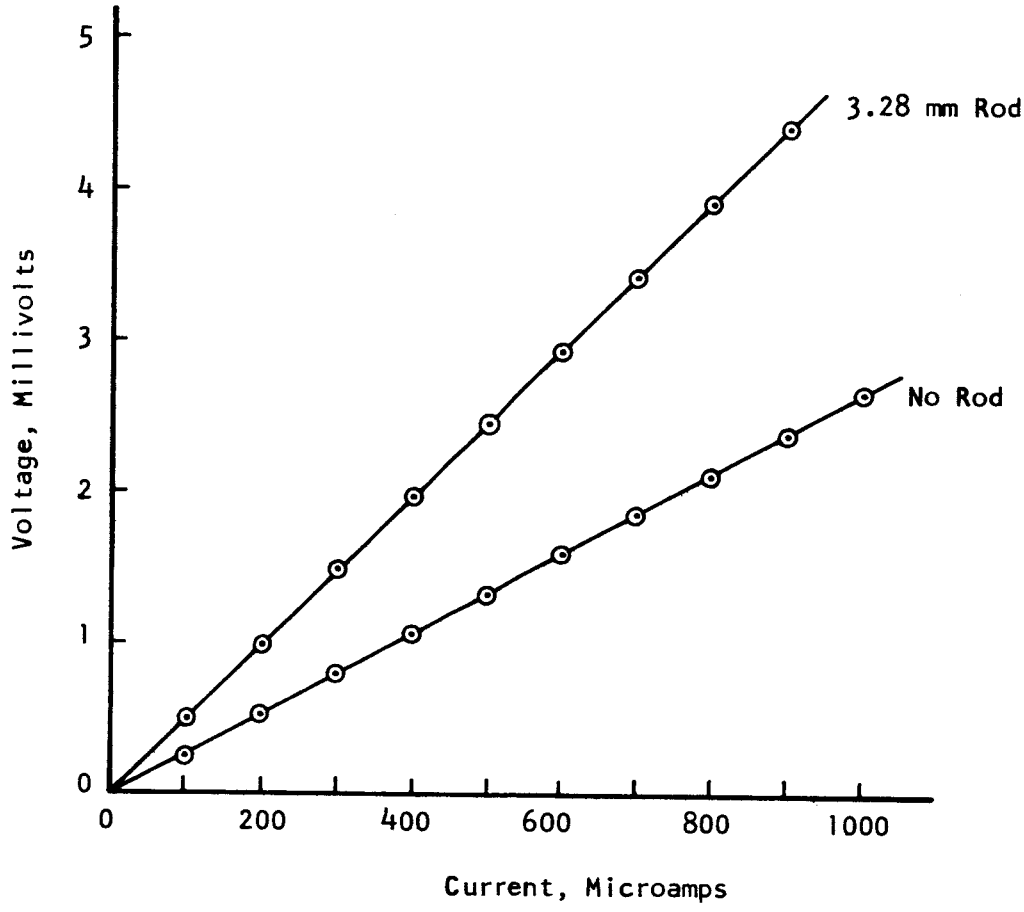

Figure 5. Voltage-Current Plot for Cell 66 Containing Mercury

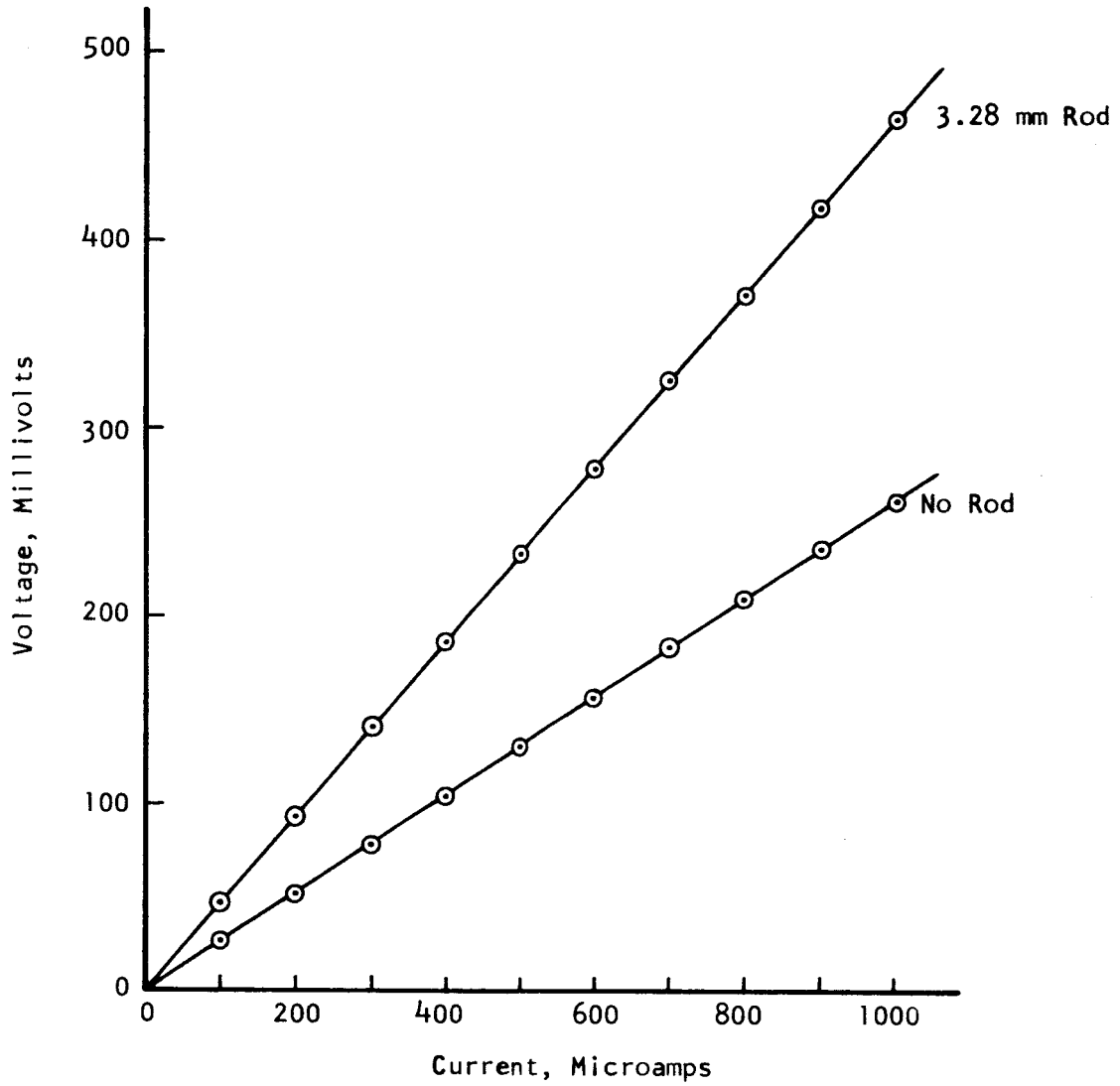

Figure 6. Voltage-Current Plot for Cell 66 Containing 1.0 N KCl

2.4 Geometrical Data on Cells 76, 74, 75

The internal diameter of the conductivity tube was measured with a small hole gage and micrometer. A cathetometer was used to measure the length of the conductivity tube L_o, and the widths of the top W_t and bottom W_b slits after the cells were completely built. The diameter of the dip rod was measured with a micrometer.

In table 3, a number of derived quantities are included for convenience since they are used in a later discussion.

TABLE 3. GEOMETRIC DATA

CELLS	76	74	75
Conductivity Tube			
Inside Diameter d_o cm	0.4727±0.0005	0.4747±0.0005	0.4762±0.0008
Length L_o cm	4.720 ±0.005	4.774 ±0.005	4.761 ±0.005
Slit Widths			
Top Slit W_t cm	0.445 ±0.005	0.045 ±0.004	0.011 ±0.005
Bottom Slit W_b cm	0.367 ±0.005	0.036 ±0.004	0.013 ±0.005
Dip Rod Diameter cm	0.4026±0.0005	0.4026±0.0005	0.4026±0.0005
Derived Quantities			
Internal Cross-sectional Area of Conductivity Tube A_o cm^2	0.1754±0.0003	0.1770±0.0003	0.1718±0.0003
Cross-Sectional Area of Dip Rod A_r cm^2	0.1273±0.0003	0.1273±0.0003	0.1273±0.0003
Average Slit Width, $\bar{W}$, cm	0.416 ±0.005	0.041 ±0.004	0.012 ±0.005
Area Ratio $\frac{A_o - A_r}{A_o}$	0.274 ±0.002	0.281 ±0.002	0.285 ±0.002
Slit Correction Factors			
Without Rod, α	0.034	0.075	0.0025
With Rod, β	0.0013	0.057	0.0023

2.5 CONDUCTIVITY DATA ON CELLS 76, 74, 75

Emf current measurements were made using both KCl and Hg with and without a dip rod inserted all the way into the cell. The experimental data for these measurements are given in table 4. Data for measurements in which position of the dip rod was varied will be reviewed in a later section.

In the present discussion we shall omit the use of the various measurements to determine effective cross-sectional areas as we did in an earlier report. The reason we did this at that time is that we were using ordinary tubing in which there are always local variations. In the present cells, precision bore tubing is used so that the problem no longer exists.

In the table it is seen that the specific conductivities determined with and without the dip rod are in poor agreement with each other if one uses L_o/A_o as the cell constant, the agreement being worse for the wider slits. We shall therefore look into the effects intorudced by the slits before proceeding further.

2.5.1 Comparison of Resistance Ratios (R_o/R_r) with Cross-sectional Area Ratios

We shall first examine the resistance ratio R_o/R_r. The advantage of this approach is that we can compare the electrical with the geometrical data fairly directly with a minimum number of parameters entering into the comparison, the specific resistivities and lengths having dropped out. An evaluation of these comparisons should enable us to localize sources of the discrepancies in the interpretation of the data. For our first examination of these data we shall take the cell constant K as equal to L_o/A_o, then

TABLE 4

SPECIFIC CONDUCTIVITIES CALCULATED FROM
ELECTRICAL RESISTANCES AND GEOMETRICAL MEASUREMENTS

CELLS		76	74	75
$\bar{W}$ cm		0.416	0.041	0.012
σ using K without end corrections, mhos/cm				
KCl	No rod	0.1081 (24°C)	0.1057 (19°C)	0.1088 (22°C)
	Rod	0.1120 (22°C)	0.1071 (19°C)	0.1070 (21°C)
Hg	No rod x 10^{-4}	1.014 (20°C)	1.045 (20°C)	1.047 (20°C)
	Rod x 10^{-4}	--	1.064 (20°C)	--
σ using K with end corrections, mhos/cm				
KCl	No rod	0.1115 (24°C)	0.1136 (19°C)	0.1092 (22°C)
	Rod	0.1121 (22°C)	0.1132 (19°C)	0.1072 (21°C)
Hg	No rod x 10^{-4}	1.048 (20°C)	1.123 (20°C)	1.049 (20°C)
	Rod x 10^{-4}	--	1.125 (20°C)	--

σ from literature, mhos/cm	20°C	25°C
1 N. KCl	0.10207	0.11180
Hg x 10^{-4}	1.0440	1.0394

$$R_o = \rho L_o / A_o,$$

$$R_r = \rho L_o / (A_o - A_r)$$

and

$$\frac{R_o}{R_r} = \frac{A_o - A_r}{A_o}$$

In table 5 we show measured ratios of R_o/R_r for both KCl and Hg as well as the ratios of the geometrical cross-sectional areas in the two sets of measurements. The agreement between the two types of measurements is poor, appearing to be worst for the widest slits.

There are several possible reasons for the discrepancy between the two sets of ratios. One is that some of the measurements are incorrect. The alternative is that the equation relating the two sets of ratios is incorrect. Since, as we have seen, the correlation between the two sets of ratios is poorest for the largest slit widths, it is probably that at least one of the sources of the discrepancy is a function of slit width. For that reason we shall make a simple derivation based on very rough assumptions to provide a first order correction to the equation for the geometrically determined cell constant. Since we are interested in establishing the nature of the problem, we shall restrict ourselves to assumptions that are reasonable and easy to apply.

Insofar as effective length is concerned, it must be greater than the length of the conductivity tube since there is a potential drop across each of the emf measuring slits rather than a single value of the potential. That is, the emf is being measured across two slits, across each of which there is an

TABLE 5

RESISTANCE RATIOS, R_o/R_r,

OF CELLS WITHOUT TO THOSE WITH DIP RODS

CELLS	76	74	75
Resistance Ratios, R_o/R_r			
KCl	0.284 ± 0.02	0.284 ± 0.05	0.280
Hg	--	0.286 ± 0.003	--
Geometrical Area Ratios			
$\frac{A_o - A_r}{A_o}$	0.274 ± 0.002	0.281 ± 0.002	0.285 ± 0.002
$\frac{A_o - A_r}{A_o} \frac{1+\alpha}{1+\beta}$	0.283	0.2856	0.2853

appreciable potential drop. The simplest approximation is to assume that the effective length terminates not at the end of the conductivity tube but in the middle of each slit. We must also make an assumption as to the effective cross-sectional area at the slit. Since the current bulges outside the cylinder at the slit, we have made the assumption that the bulge is approximately semi-circular and that the effective average radius in this region can be taken as the sum of the conductivity tube radius plus $1/\sqrt{2}$ of the radius of the circular bulge. In carrying out this analysis we are ignoring perturbations inside the conductivity tube in the neighborhood of the slit. Hence, the corrections are rough, but we shall see that they appear to be adequate to account for the resistance ratios.

Continuing the derivation, we shall assume that resistances in series are additive, that is, that

$$R = \rho \sum \frac{L_i}{A_i}$$

This cannot be strictly correct in any of the transition regions in the cell. However, using this assumption, we obtain the following two equations.

$$R_o = \rho \frac{L_o}{A_o} \left[1 + \frac{\bar{w}}{L_o} \frac{1}{\left(1 + \frac{\bar{w}}{\sqrt{2}\, d_o}\right)^2} \right]$$

$$= \rho \frac{L_o}{A_o} (1 + \alpha)$$

and

$$R_r = \rho \frac{L_o}{A_o - A_r} \left[1 + \frac{\bar{W}}{L_o} \frac{A_o - A_r}{A_o \left(1 + \frac{\bar{W}}{\sqrt{2}\, d_o}\right)^2 - A_r} \right]$$

$$= \rho \frac{L_o}{A_o - A_r} (1 + \beta)$$

We have tabulated the values of α and β in table 3. Using these, we obtain a correction term for the resistance ratio

$$\frac{R_o}{R_r} = \frac{A_o - A_r}{A_o} \frac{1 + \alpha}{1 + \beta}$$

It is seen in table 5 that the agreement between the resistance ratios and effective area ratios corrected for the slit effects is excellent. The slit effects therefore account for the differences between the resistance ratios and uncorrected area ratios quantitatively.

2.5.2 Specific Conductivities

On table 3 we saw that there were discrepancies between specific conductivities using geometrical cell constants without end corrections. In the last section we showed that a simple correction is adequate for purposes of accounting for resistance ratios. In this comparison, the specific conductivities and effective lengths drop out, so that we must examine to see whether the corrections applied therein are equally valid and useful when applied to the system as a whole. For that reason, in table 4 we give the specific conductivities for KCl and Hg, with and without dip rod, calculated with and without end corrections.

It is seen that the simple end effect corrections are adequate to remove the discrepancies between cells with and without rods. However, the data for both Hg and KCl are in poor accord with the specific conductivities in the literature. This may occur for at least one of two reasons: either the corrections applied to the data are not adequate, or there is an appreciable temperature rise in the conductivity tube during the measurements due to ohmic heating.

2.5.3 Discrepancies

When we applied the end effect corrections derived for resistance ratios to the specific conductivities, we eliminated one type of discrepancy (that between cells with and without dip rods), but a new one arose; namely, the values of specific conductivities for both KCl and Hg became larger than those in the literature. There are at least three possible sources which can give rise to this discrepancy. One is that KCl and Hg may have impurities or there may be an error in the KCl concentration. A second is that there may be sufficient ohmic heating to change the temperatures of the liquids in the conductivity tube and hence their specific conductivities. A third is that, although the end effect correction gave excellent results with respect to the relative cross-sectional areas, the present discrepancy may be due to its giving poor results when correcting for the behavior of the cell as a whole.

If ohmic heating is responsible for the remaining discrepancies, then with increase in temperature the specific conductivity of KCl should increase whereas that for Hg should decrease. This is not in accord with the data

since both increase. Hence, ohmic heating effects are not the principal cause of the discrepancy. Therefore, we must determine whether the discrepancy is due to our materials having wrong specific conductivities or whether the correction factors are inadequate for the overall cell.

In the following section we examine variable dip rod data. These results give us an independent approach to distinguish between the remaining two sources of the discrepancy. It will be seen that the variable dip rod results give specific conductivities in better agreement with the literature than the conductivities corrected for end effects. This indicates that the principal difficulty is not the presence of impurities or wrong concentrations but rather that the functions $1 + \alpha$ and $1 + \beta$ are in error.

Once we have established this, then it is no longer important to treat the correction problem further since our main use of the correction factor is to establish a maximum slit width such that we can ignore the corrections and to provide an understanding of the way the cell operates.

2.6 VARIABLE POSITION DIP ROD

In the dip rod technique, the rod is lowered to various positions in the conductivity tube, and the voltage across this tube is measured at constant current. KCl has one advantage over Hg, in that it is transparent so that one may visually observe the position of the rod with respect to the ends of the conductivity tube and the slits. A typical curve of voltage vs. position of the bottom end of the rod is given in Fig. 7. There are three side effects; namely, (1) the curve is not linear in the neighborhood of the slits, (2) the curve, if drawn linearly, does not intersect the two base curves at the edges of the conductivity tube, and (3) both intersections are displaced downward, the displacement being larger at the upper slit.

In the region where the dip rod data are well behaved, the interpretation of the data appears to be clear cut. We shall restrict the derivation to the case where the end of the rod is not near either edge of the conductivity tube.

When the dip rod is in position in the cell, the emf measuring circuit contains at least five different regions. In three of these regions, A, C, E (i.e., in the neighborhood of the two slits and the end of the rod), the current distribution is not uniform. In this derivation we shall assume that as long as the end of the rod is not near either edge of the conductivity tube, the current distributions in each of these three regions remains unaltered.

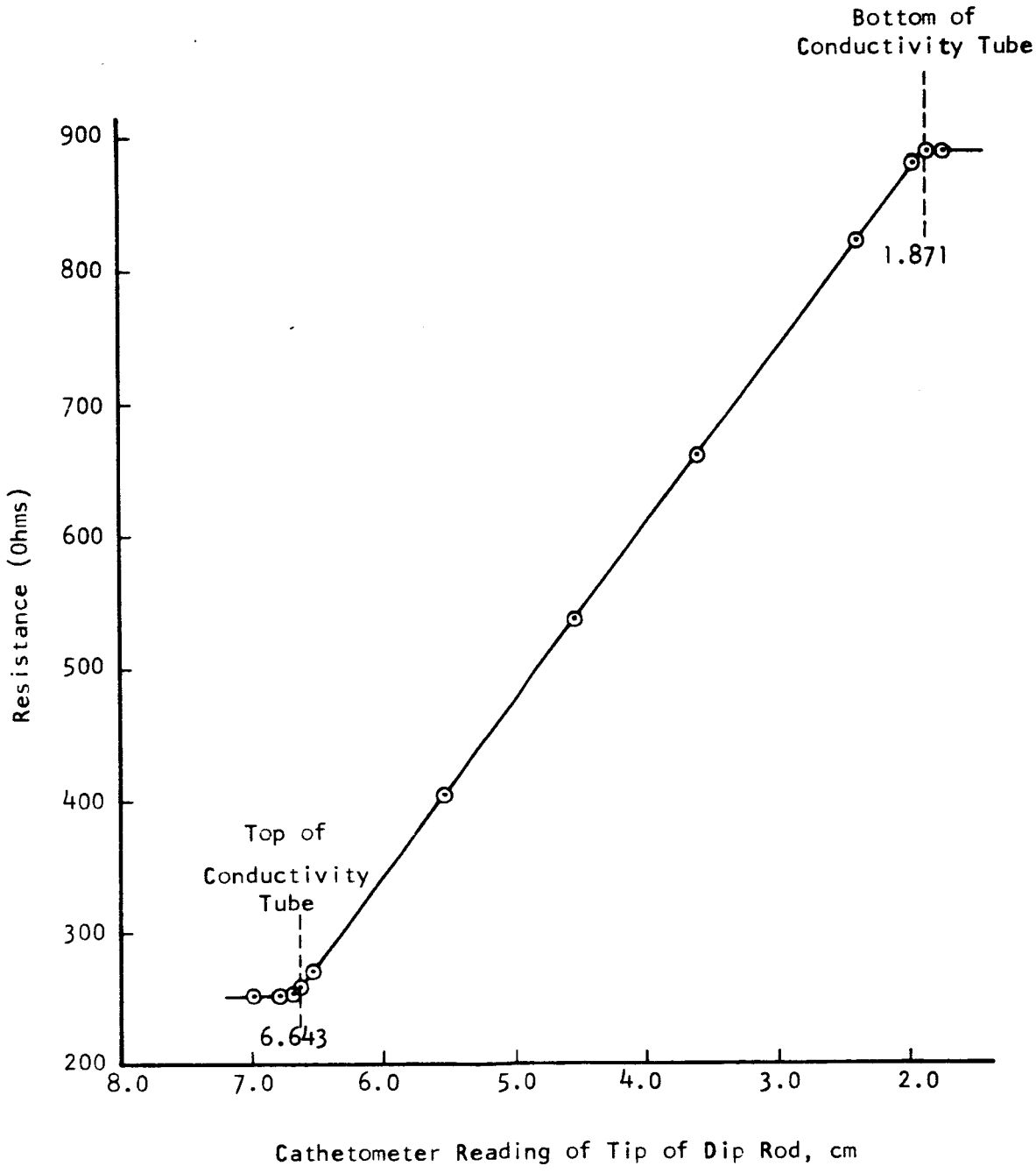

Figure 7. Resistance vs Rod Depth in the Conductivity Tube of Cell 74, Using 1.0 N KCl Solution as Conducting Liquid

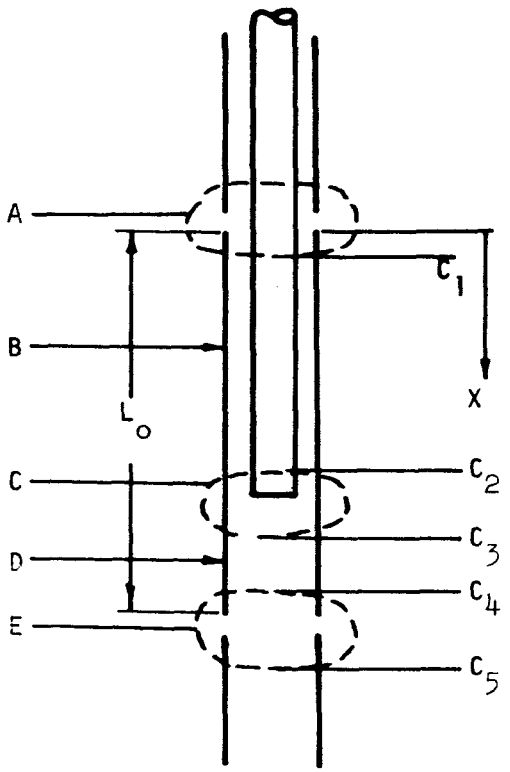

The widths of these regions are not important as long as they are constant, since the derivatives of the voltages with respect to the position of the end of the rod are then zero for these regions.

Let x be the position of the end of the rod below the upper edge of the conductivity tube. Let c_1, c_2, c_3, c_4, be the distances to the edges of the three non-uniform regions, as shown. The measured resistance in the conductivity tube is

$$R = R_A + R_B + R_C + R_D + R_E$$

Differentiating with respect to the position of the tip of the rod, x, we obtain

$$\frac{dR}{dx} = \frac{dR_B}{dx} + \frac{dR_D}{dx}$$

the other terms drop out since, by assumption, they are independent of the position of the end of the rod as long as the rod is not near the edges of the conductivity tube. Since

$$R_B = \rho \frac{L_B}{A_B} = \rho \frac{(x - c_2) - c_1}{A_o - A_r}$$

and

$$R_D = \rho \frac{(L_o - c_4) - (x + c_3)}{A_o}$$

then

$$\frac{dR}{dx} = \frac{\rho}{A_o - A_r} - \frac{\rho}{A_o} = \rho \frac{A_r}{A_o(A_o - A_r)}$$

Since we measure emfs, and since the current, i, is constant, the partial derivative of voltage with respect to rod position, S_x, is given by

$$S_x = (\partial E/\partial x)_i = i\, dR/dx,$$

and

$$\sigma = \frac{i}{S_x} \frac{A_r}{A_o(A_o - A_r)}$$

Basically, we have substituted measurements of voltage as a function of position for those of length. In doing this, we have avoided the end regions for which corrections must otherwise be applied.

The data for the variable dip rod technique are summarized in table 6. The results for cell 76 are worse by 7% than those with end corrections (table 4, page 22). There is a distinct improvement in results for cell 74 both for KCl and Hg, there being a 4% improvement for KCl and a 6% improvement for Hg. For cell 75, the results are slightly worse (1%).

Comparing the variable dip rod data, the discrepancy for cell 76 indicates that our simple treatment is not adequate for very wide slits and that a more sophisticated analysis may be needed. The consistency of cells 74 and 75 is good, far better than for the results in table 3. This indicates that part of the trouble with the results therein is due to the corrections used.

TABLE 6. VARIABLE DIP ROD DATA

CELLS	76	74	75
Average Slit Widths $\bar{W}$ cm	0.416	0.041	0.012
Tangent S_x/i ohms/cm			
KCl	127	133	130
Hg	--	1.357×10^{-3}	--
σ from Tangents, mhos/cm			
KCl	0.119	0.109	0.109
Hg	--	1.066×10^{4}	--

If one examines the data for the cell with the narrowest slits (75), one sees that the data are generally quite consistent. In particular, the end

effect corrections are small, amounting to 0.4%, and the variable dip rod technique agrees within 1% with the specific conductivities.

From this we conclude that the straight geometrical measurements will give acceptable values of the cell constants to 1% for slit widths of or less than 0.01 cm. A discrepancy remains between our values of specific conductivities and those in the literature, but agreement has been obtained between specific conductivity determined by two independent approaches.

3.0 PRESSURE SYSTEM

The presence of leaks in a valve and several fittings made it impossible to operate at pressures over 100 atmospheres for more than a few hours during the early part of the quarter. As the bomb thermal equilibrium time was from 12 to 24 hours, we were unable to run to temperatures over 100°C (100 atmospheres).

The bomb was dismantled and cleaned. A new valve, fittings, cell leads and seals, as well as a new ceramic liner, were installed. Along with cleaning the bomb and its high pressure lines, some system modifications have been made to eliminate unnecessary fittings and joints. To prevent future contamination of the system, the cells are wrapped in teflon sheet that will hold loose amalgam.

Leak rate measurements before the recent failure show an average pressure loss of 0.5 atm. per hour at 300 atmospheres (4500 psia) at that time. This rate was low enough to allow us to run cells overnight at elevated temperatures without fear of a pressure drop causing them to explode.

The bomb failure described in section 1 occurred at the end of this quarter and was caused by electrochemical attack of the coolant tube by amalgam residues with slight shorting of the heater providing the energy. This attack ate a 1/16 inch diameter hole in the 0.062 wall stainless steel coolant tube. The tube, which is embedded in ceramic, will be patched with a stainless steel plug and oven dried at 200°C to prevent future attack. This repair will necessitate replacing much of the mounting ceramic and will allow inspection of part of the coolant tube for other points of attack.

4.0 PROGRAM FOR NEXT QUARTER

Repairs on the pressure bomb will be completed and one more amalgam concentration cell will be run. This cell, like cell 64, will be treated with ultrasonic agitation in order to insure electrode uniformity.

Six cells with amalgam-insoluble electrodes of known compositions have been fabricated. These cells will be filled using Pb, Cd, Z and Tl amalgam-insoluble salt electrodes. These cells will then be run.

OFFICIAL DISTRIBUTION LIST
FOR BATTERY REPORTS

March 10, 1966

NASA and JPL

National Aeronautics & Space Admin.
Scientific and Technical Information Facility
College Park, Maryland 20740
Attn: NASA Representative
Send 2 copies plus 1 reproducible

National Aeronautics & Space Admin.
Washington, D.C. 20546
Attn: RNW/E.M. Cohn

National Aeronautics & Space Admin.
Washington, D.C. 20546
Attn: FC/A. M. Greg Andrus

National Aeronautics & Space Admin.
Goddard Space Flight Center
Greenbelt, Maryland 20771
Attn: Thomas Hennigan, Code 716.2

National Aeronautics & Space Admin.
Goddard Space Flight Center
Greenbelt, Maryland 20771
Attn: Joseph Sherfey, Code 735

National Aeronautics & Space Admin.
Langley Research Center
Instrument Research Division
Hampton, Virginia 23365
Attn: John L. Patterson, MS-234

National Aeronautics & Space Admin.
Langley Research Center
Instrument Research Division
Hampton, Virginia 23365
Attn: M. B. Seyffert, MS 112

National Aeronautics & Space Admin.
Lewis Research Center
21000 Brookpark Road
Cleveland, Ohio 44135
Attn: N. D. Sanders, MS 302-1

National Aeronautics & Space Admin.
Lewis Research Center
21000 Brookpark Road
Cleveland, Ohio 44135
Attn: R. L. Cummings, MS 500-201

National Aeronautics & Space Admin.
Lewis Research Center
21000 Brookpark Road
Cleveland, Ohio 44135
Attn: R. R. Miller, MS 500-202

National Aeronautics & Space Admin.
Geo. C. Marshall Space Flight Center
Huntsville, Alabama 35812
Attn: Philip Youngblood

National Aeronautics & Space Admin.
Geo. C. Marshall Space Flight Center
Huntsville, Alabama 35812
Attn: Richard Boehme
Bldg. 4487-BB

National Aeronautics & Space Admin.
Manned Spacecraft Center
Houston, Texas 77058
Attn: William R. Dusenbury
Propulsion & Energy Systems Branch
Bldg. 16, Site 1

National Aeronautics & Space Admin.
Manned Spacecraft Center
Houston, Texas 77058
Attn: Robert Cohen
Gemini Project Office

National Aeronautics & Space Admin.
Manned Spacecraft Center
Houston, Texas 77058
Attn: Richard Ferguson (EP-5)

National Aeronautics & Space Admin.
Manned Spacecraft Center
Houston, Texas 77058
Attn: James T. Kennedy (EE-5)

National Aeronautics & Space Admin.
Manned Spacecraft Center
Houston, Texas 77058
Attn: Forrest E. Eastman (EE-4)

National Aeronautics & Space Admin.
Ames Research Center
Pioneer Project
Moffett Field, California 94035
Attn: James R. Swain/A. S. Hertzog

National Aeronautics & Space Admin.
Ames Research Center
Moffett Field, California 94035
Attn: Jon Rubenzer
Biosatellite Project

Jet Propulsion Laboratory
4800 Oak Grove Drive
Pasadena, California 91103
Attn: Aiji Uchiyama

Department of the Army

U. S. Army Engineer R&D Labs.
Fort Belvoir, Virginia 22060
Electrical Power Branch
SMCFB-EP

Commanding Officer
U. S. Army Electronics R&D Labs.
Forth Monmouth, New Jersey 07703
Attn: Power Sources Division
Code SELRA/PS

Research Office
Rand D. Directorate
Army Weapons Command
Rock Island, Illinois 61201
Attn: Mr. G. Riensmith, Chief

U. S. Army Research Office
Box CM, Duke Station
Durham, North Carolina 27706
Attn: Dr. Wilhelm Jorgensen

Natick Laboratories
Clothing and Organic Materials Div.
Natick, Massachusetts 01760
Attn: Robert N. Walsh/G. A. Spano

Harry Diamond Laboratories
Room 300, Building 92
Conn.Ave. & Van Ness Street, N.W.
Washington, D.C. 20438
Attn: Nathan Kaplan

Army Materiel Command
Research Division
AMCRD-RSCM-T-7
Washington, D.C. 20315
Attn: John W. Crellin

Army Materiel Command
Development Division
AMCRD-DE-MO-P
Washington, D.C. 20315
Attn: Marshall D. Aiken

U.S. Army TRECOM
Fort Eustis, Virginia 23604
Attn: Dr. R. L. Echols (SMOFE-PSG)

U. S. Army TRECOM
Fort Eustis, Virginia 23604
Attn: Leonard M. Bartone (SMOFE-ASE)

U. S. Army Mobility Command
Research Division
Center Line, Michigan 48090
Attn: O. Renius (AMSMO-RR)

Department of the Navy

Office of Naval Research
Washington, D.C. 20360
Attn: Head, Power Branch, Code 429

Office of Naval Research
Department of the Navy
Washington, D.C. 20360
Attn: H. W. Fox, Code 425

Naval Research Laboratory
Washington, D.C. 20390
Attn: Dr. J. C. White, Code 6160

U. S. Navy
Marine Engineering Laboratory
Annapolis, Maryland 21402
Attn: J. H. Harrison

Bureau of Naval Weapons
Department of the Navy
Washington, D.C. 20360
Attn: Whitewell T. Beatson
(Code RAAE-52)

Bureau of Naval Weapons
Department of the Navy
Washington, D.C. 20360
Attn: Milton Knight (Code RAAE-50)

Naval Ammunition Depot
Crane, Indiana 47522
Attn: E. Bruess/H. Shultz

Naval Ordnance Laboratory
Department of the Navy
Corona, California 91720
Attn: William C. Spindler (Code 441)

Naval Ordnance Laboratory
Department of the Navy
Silver Spring, Maryland 20900
Attn: Philip B. Cole (Code WB)

Bureau of Ships
Department of the Navy
Washington, D.C. 20360
Attn: C. F. Viglotti (Code 660)

Bureau of Ships
Department of the Navy
Washington, D.C. 20360
Attn: Bernard B. Rosenbaum (Code 340)

Department of the Air Force

Space Systems Division
Los Angeles AF Station
Los Angeles, California 90045
Attn: SSSD

Flight Vehicle Power Branch
Aero Propulsion Laboratory
Wright-Patterson AFB, Ohio 45433
Attn: James E. Cooper

Air Force Cambridge Research Lab.
L. G. Hanscom Field
Bedford, Massachusetts 01731
Attn: Commander (CRO)

Rome Air Development Center, ESD
Griffis AFB, New York 13442
Attn: Frank J. Mollura (RASSM)

Other Government Agencies

National Bureau of Standards
Washington, D.C. 20234
Attn: Dr. W. J. Hamer

Office, DDR&E, USE & BSS
The Pentagon
Washington, D.C. 20310
Attn: G. B. Wareham

Mr. Donald B. Hoatson
Army Reactors, DRD
U. S. Atomic Energy Commission
Washington, D.C. 20545

Private Organizations

Aeroject-General Corporation
Chemical Products Division
Azusa, California 91702
Attn: Dr. S. O. Rosenberg

Aeronutronic Division
Philco Corporation
Ford Road
Newport Beach, California 92660

Aerospace Corporation
P.O. Box 95085
Los Angeles, California 90045
Attn: Library

Allis-Chalmers Manufacturing Co.
1100 South 70th Street
Milwaukee, Wisconsin 53201
Attn: Dr. P. Joyner

American University
Mass. & Nebraska Avenues, N.W.
Washington, D.C. 20016
Attn: Dr. R. T. Foley,
Chemistry Department

Arthur D. Little, Inc.
Acorn Park
Cambridge, Massachusetts 02140
Attn: Dr. Ellery W. Stone

Atomics International Division
North American Aviation, Inc.
8900 De Sota Avenue
Canoga Park, California 91304
Attn: Dr. H. L. Recht

Battelle Memorial Institute
505 King Avenue
Columbus, Ohio 43201
Attn: Dr. C. L. Faust

Bell Laboratories
Murray Hill, New Jersey 07971
Attn: U. B. Thomas/D. A. Feder

The Boeing Company
P. O. Box 98124
Seattle, Washington 98124

Borden Chemical Company
Central Research Lab.
P. O. Box 9524
Philadelphia, Pennsylvania 19124

Burgess Battery Company
Foot of Exchange Street
Freeport, Illinois 61032
Attn: Dr. Howard J. Strauss

C & D Batteries
Division of Electric Autolite Co.
Conshohocken, Pennsylvania 19428
Attn: Dr. Eugene Willihnganz

Calvin College
Grand Rapids, Michigan 49506
Attn: Prof. T. P. Dirkse

Catalyst Research Corporation
6101 Falls Road
Baltimore, Maryland 21209
Attn: J. P. Wooley

ChemCell Inc.
3 Central Avenue
East Newark, N.J. 07029
Attn: Peter D. Richman

Delco Remy Division
General Motors Corporation
2401 Columbus Avenue
Anderson, Indiana 46011
Attn: Dr. J. J. Lander

Douglas Aircraft Company, Inc.
Astropower Laboratory
2121 Campus Drive
Newport Beach, California 92663
Attn: Dr. Carl Berger

Dynatech Corporation
17 Tudor Street
Cambridge, Massachusetts 02138
Attn: R. L. Wentworth

Eagle-Picher Company
Post Office Box 47
Joplin, Missouri 64802
Attn: E. M. Morse

Elgin National Watch Company
107 National Street
Elgin, Illinois 60120
Attn: T. Boswell

Electric Storage Battery Co.
Missile Battery Division
2510 Louisburg Rd.
Raleigh, North Carolina 27604
Attn: A. Chreitzberg

Electric Storage Battery Co.
Carl F. Norberg Research Center
19 West College Avenue
Yardley, Pennsylvania 19068
Attn: Dr. R. A. Schaefer/W. S. Herbert

Electrochimica Corporation
1140 O'Brien Drive
Menlo Park, California 94025
Attn: Dr. Morris Eisenberg

Electro-Optical Systems, Inc.
300 North Halstead
Pasadena, California 91107
Attn: E. Findl

Emhart Manufacturing Co.
Box 1620
Hartford, Connecticut 06101
Attn: Dr. W. P. Cadogan

Engelhard Industries, Inc.
497 DeLancy Street
Newark, New Jersey 07105
Attn: Dr. J. G. Cohn

Dr. Arthur Fleischer
466 South Center Street
Orange, New Jersey 07050

General Electric Company
Schenectady, New York, 12301
Attn: Dr. R. C. Osthoff/Dr. W. Carson
Advanced Technology Lab.

General Electric Company
Missile & Space Division
Spacecraft Department
P. O. Box 8555
Philadelphia, Pennsylvania 19101
Attn: E. W. Kipp, Room T-2513

General Electric Company
Battery Products Section
P. O. Box 114
Gainsville, Florida 32601

General Electric Company
Research Laboratories
Schenectady, New York 12301
Attn: Dr. H. Liebhafsky

General Motors-Defense Research Labs.
6767 Hollister Street
Santa Barbara, California 93105
Attn: Dr. J.S. Smatko/Dr. C. R. Russell

Globe-Union, Incorporated
900 East Keefe Avenue
Milwaukee, Wisconsin 53201

Gould-National Batteries, Inc.
Engineering and Research Center
2630 University Avenue, S.E.
Minneapolis, Minnesota 55418
Attn: J. F. Donahue

Gulton Industries
Alkaline Battery Division
212 Durham Avenue
Metuchen, New Jersey 08840
Attn: Dr. Robert Shair

Hughes Aircraft Corporation
Centinda Ave. & Teale St.
Culver City, California 90230
Attn: T. V. Carvey

Hughes Aircraft Corporation
Bldg. 366, M.S. 524
El Segundo, California 90245
Attn: R. B. Robinson

Hughes Research Laboratories Corp.
3011 Malibu Canyon Rd.
Malibu, California 90265

ITT Research Institute
10 West 35th Street
Chicago, Illinois 60616
Attn: Dr. H. T. Francis

Institute for Defense Analyses
R&E Support Division
400 Army-Navy Drive
Arlington, Virginia 22202
Attn: Mr. R. Hamilton/Dr. Szego

Idaho State University
Department of Chemistry
Pocatello, Idaho 83201
Attn: Dr. G. Myron Arcand

Institute of Gas Technology
State and 34th Street
Chicago, Illinois 60616
Attn: B. S. Baker

Johns Hopkins University
Applied Physics Laboratory
8621 Georgia Avenue
Silver Spring, Maryland 20910
Attn: Richard Cole

Johns-Manville R&E Center
P.O. Box 159
Manville, New Jersey 08835
Attn: J. S. Parkinson

Leesona Moos Laboratories
Lake Success Park, Community Drive
Great Neck, New York 11021
Attn: Dr. H. Oswin

Livingston Electronic Corporation
Route 309
Montgomeryville, Pennsylvania 18936
Attn: William F. Meyers

Lockheed Missiles & Space Company
3251 Hanover Street
Palo Alto, California 93404
Attn: Library

Mallory Battery Company
60 Elm Street
North Tarryton, New York 10593
Attn: R. R. Clune

P. R. Mallory & Co., Inc.
Northwest Industrial Park
Burlington, Massachusetts 02103
Attn: Dr. Per Bro

P. R. Mallory & Co., Inc.
3029 E. Washington Street
Indianapolis, Indiana 46206
Attn Technical Librarian

Melpar
Technical Information Center
3000 Arlington Blvd.
Falls Church, Virginia 22046

Metals and Controls Division
Texas Instruments, Inc.
34 Forest Street
Attleboro, Massachusetts 02703
Attn: Dr. E. M. Jost

Midwest Research Institute
425 Volker Boulevard
Kansas City, Missouri 64110
Attn: Dr. B. W. Beadle

Monsanto Research Corporation
Everett, Massachusetts 02149
Attn: Dr. J. O. Smith

North American Aviation, Inc.
Rocketdyne Division
6633 Canoga Avenue
Canoga Park, California 91303
Attn: Library

North American Aviation, Inc.
12214 Lakewood Boulevard
Downey, California 90241
Attn: Burton M. Otzinger

Dr. John Owen
P. O. Box 87
Bloomfield, New Jersey 07003

Power Information Center
University of Pennsylvania
Moore School Building
200 South 33rd Street
Philadelphia, Pennsylvania 19104

Power Sources Division
Whittaker Corporation
9601 Canoga Avenue
Chatsworth, California 91311
Attn: Dr. M. Shaw

Philco Corporation
Division of the Ford Motor Co.
Blue Bell, Pennsylvania 19422
Attn: Dr. Phillip Cholet

Radiation Applications, Inc.
36-40 37th Street
Long Island City, New York 11101

Radio Corporation of America
Astro Division
Hightstown, New Jersey 08520
Attn: Seymour Winkler

Radio Corporation of American
P. O. Box 800
Princeton, New Jersey 08540
Attn: I. Schulman

Radio Corporation of America
Somerville, New Jersey 08873
Attn: Dr. H. S. Lozier

Southwest Research Institute
8500 Culebra Road
San Antonio, Texas 78206
Attn: Dr. Jan Al

Sonotone Corporation
Saw Mill River Road
Elmsford, New York 10523
Attn: A. Mundel

Texas Instruments, Inc.
13500 North Central Expressway
Dallas, Texas 75222
Attn: Dr. Isaac Trachtenberg

Thomas A. Edison Research Laboratory
McGraw Edison Company
Watchung Avenue
West Orange, New Jersey 07052
Attn: Dr. P. F. Grieger

TRW Systems, Inc.
One Space Park
Redondo Beach, California 90278
Attn: Dr. A. Krausz, Bldg. 60, Rm 929

TRW Systems Inc.
One Space Park
Redondo Beach, California 90278
Attn: Dr. Herbert P. Silverman

TRW, Inc.
23555 Euclid Avenue
Cleveland, Ohio 44117
Attn: Librarian

Tyco Laboratories, Inc.
Bear Hill
Hickory Drive
Waltham, Massachusetts 02154
Attn: W. W. Burnett

Union Carbide Corporation
Development Laboratory Library
P. O. Box 6056
Cleveland, Ohio 44101

Union Carbide Corporation
Parma Research Center
P. O. Box 6116
Cleveland, Ohio 44101
Attn: Library

University of California
Space Science Laboratory
Berkeley, California 94720
Attn: Dr. C. W. Tobias

University of Pennsylvania
Electrochemistry Laboratory
Philadelphia, Pennsylvania 19104

Western Electric Company
Suite 802, RCA Bldg.
Washington, D.C. 20006
Attn: R. T. Fiske

Westinghouse Electric Corporation
Research & Development Center
Churchill Borough
Pittsburgh, Pennsylvania 15235

Whittaker Corporation
P. O. Box 337
Newbury Park, California 91320
Attn: Mr. John Rhyne

Whittaker Corporation
3850 Olive Street
Denver, Colorado 80237
Attn: Borch Wendir

Yardney Electric Corporation
40-50 Leonard Street
New York, New York 10013
Attn: Dr. Geo. Dalin